

## Video Article

# High-frequency Ultrasound Imaging of Mouse Cervical Lymph Nodes

Elyse L. Walk<sup>\*1,3</sup>, Sarah L. McLaughlin<sup>\*2,3</sup>, Scott A. Weed<sup>1,3</sup><sup>1</sup>Department of Neurobiology and Anatomy, West Virginia University<sup>2</sup>Animal Models and Imaging Facility, West Virginia University<sup>3</sup>Mary Babb Randolph Cancer Center, West Virginia University

\*These authors contributed equally

Correspondence to: Scott A. Weed at [scweed@hsc.wvu.edu](mailto:scweed@hsc.wvu.edu)URL: <https://www.jove.com/video/52718>DOI: [doi:10.3791/52718](https://doi.org/10.3791/52718)

Keywords: Medicine, Issue 101, Ultrasound, cervical lymphnode, mouse, imaging, animal model, anatomy, mapping.

Date Published: 7/25/2015

Citation: Walk, E.L., McLaughlin, S.L., Weed, S.A. High-frequency Ultrasound Imaging of Mouse Cervical Lymph Nodes. *J. Vis. Exp.* (101), e52718, doi:10.3791/52718 (2015).

## Abstract

High-frequency ultrasound (HFUS) is widely employed as a non-invasive method for imaging internal anatomic structures in experimental small animal systems. HFUS has the ability to detect structures as small as 30  $\mu\text{m}$ , a property that has been utilized for visualizing superficial lymph nodes in rodents in brightness (B)-mode. Combining power Doppler with B-mode imaging allows for measuring circulatory blood flow within lymph nodes and other organs. While HFUS has been utilized for lymph node imaging in a number of mouse model systems, a detailed protocol describing HFUS imaging and characterization of the cervical lymph nodes in mice has not been reported. Here, we show that HFUS can be adapted to detect and characterize cervical lymph nodes in mice. Combined B-mode and power Doppler imaging can be used to detect increases in blood flow in immunologically-enlarged cervical nodes. We also describe the use of B-mode imaging to conduct fine needle biopsies of cervical lymph nodes to retrieve lymph tissue for histological analysis. Finally, software-aided steps are described to calculate changes in lymph node volume and to visualize changes in lymph node morphology following image reconstruction. The ability to visually monitor changes in cervical lymph node biology over time provides a simple and powerful technique for the non-invasive monitoring of cervical lymph node alterations in preclinical mouse models of oral cavity disease.

## Video Link

The video component of this article can be found at <https://www.jove.com/video/52718/>

## Introduction

Lymph drainage of interstitial tissue fluid is the main method of dissemination for infectious microorganisms and cancers arising in the oral and maxillofacial region<sup>1,2</sup>. Clinical evaluation of cervical lymph nodes is a common diagnostic practice used to determine the presence or progression of diseases that originate in the oral cavity. This underscores the importance of the collecting cervical lymph nodes as valuable anatomic sites for oral disease diagnosis<sup>3</sup>. Several specialized imaging methodologies are clinically utilized for identifying diseased cervical lymph nodes. These include positron emission tomography (PET), computed tomography (CT) and magnetic resonance imaging (MR). While highly valuable, these methods all require extensive patient preparation, highly specialized equipment and/or chemical infusion into the circulation to enable or enhance the imaging process.

Sonographic imaging (ultrasound; US) is a commonly applied technique used to image cervical lymph nodes presenting with lymphadenopathy due to infection or metastatic involvement<sup>4-6</sup>. US is often combined with PET-CT and MR imaging to provide a comprehensive representation of patient lymph node status, helping to determine tumor staging and necessity for surgical excision<sup>7</sup>. The non-invasive nature of US also has inherent advantages over other imaging modalities, including ease of use, low cost, minimal patient discomfort and preparation. The superficial subcutaneous location of most cervical lymph nodes allows for US to guide minimally invasive fine needle aspiration biopsies with increased precision, improving diagnostic accuracy<sup>8</sup>.

Commercial high-frequency (HF) US provides detailed resolution of internal anatomic structures to 30  $\mu\text{m}$ <sup>9</sup>. Using transducers ranging from 22-70 MHz, HFUS has been readily applied to a variety of experimental rodent systems to allow real-time imaging of internal organs in vivo. HFUS has been adapted for visualization of tumor formation in conventional brightness (B)-mode, as well as with a number of general and specialized contrast enhancement agents<sup>9</sup>. Using power Doppler with HFUS provides the ability to monitor blood flow within mouse tumors, allowing a comprehensive assessment of angiogenic perfusion in live mice<sup>10,11</sup>. HFUS has been used to visualize diseased mouse lymph nodes within the main body cavity, demonstrating parallel utility of this technology to clinical practice. In particular, inflammatory and metastatic visceral lymph node alterations have been observed in mouse models of cancer harboring breast<sup>12,13</sup>, pancreatic<sup>14</sup>, colorectal<sup>15</sup> and lung<sup>16</sup> tumors, as well as fibrous histiocytomas<sup>17</sup>, and an aged mouse model of acquired hydronephrosis<sup>18</sup>. These examples solidify the value of HFUS as a powerful investigative tool for tumor-induced lymphadenopathy in a wide variety of rodent systems.

Several models of bacterial infection<sup>19,20</sup> and head and neck squamous cell carcinoma (HNSCC)<sup>21,22</sup> have been developed to study these diseases in the preclinical setting. In contrast to humans, mice contain three cervical lymph nodes that survey lymph from oral cavity tissues (mandibular, submandibular mandibular and superficial parotid<sup>23</sup>). Recently, we reported the use of HFUS to map the location and morphology of these lymph nodes, monitoring changes in lymph node volume and blood flow in a carcinogen-induced mouse model of HNSCC<sup>24</sup>. Here, we provide a detailed protocol for the use of HFUS for identifying, imaging and analyzing cervical lymph nodes in living mice. This protocol also demonstrates the feasibility of using HFUS to conduct image-guided fine needle biopsy of enlarged mouse cervical lymph nodes, allowing histological monitoring of changes in cervical lymph node content and pathologies over time in the same animal. This protocol is readily adaptable to allow for the detailed study of cervical lymph node pathologies resultant from any invasive oral cavity disease in mice.

## Protocol

All animal procedures demonstrated in this protocol have been reviewed and approved by the West Virginia University Animal Care and Use Committee under protocols 11-0412 and 14-0514 and conducted in accordance with the principles and procedures outlined in the NIH Guide for the Care and Use of Animals.

### 1. Animal Preparation

1. Anesthetize a single mouse in an induction chamber using 3% isoflurane mixed with 1.5 L/min 100% oxygen. Remove the animal from the induction chamber and place in a supine position on the imaging platform preheated to 40 °C and maintained between 37-42 °C (**Figure 2A**). Confirm anesthesia by the lack of response to a toe pinch.
2. Position the mouse snout within the nosecone connected to the anesthesia system. Apply anesthesia to maintain steady state sedation (1.5% isoflurane mixed with 1.5 L/min 100% oxygen).
3. Apply eye lubricant the each eye to prevent drying. Apply electrode gel to the electrodes and use tape to secure each of the four paws to the corresponding electrode. The electrode pads will transmit the animal's ECG to the imaging system to allow monitoring of heart rate and respiration rate. Lubricate and insert the rectal temperature probe for continuous monitoring of body temperature. Normal mouse body temperature is 36.9 °C. 1-2 °C variation is normal while under anesthesia.
4. Use depilatory cream to remove the fur from the neck of the mouse. Rinse the neck region with water-soaked gauze to remove hair and excess depilatory cream. Optionally, use additional application of depilatory cream to remove any remaining body hair (**Figure 2B**).

### 2. Identification and Image Acquisition of Mouse Cervical Lymph Nodes Using HFUS

1. To begin, apply a layer of warmed ultrasound gel to the neck area devoid of fur. Use liberal application of gel for optimal image quality (**Figure 2C**). Avoid introducing air bubbles in the gel during application, which can interfere with ultrasonic imaging.
2. Adjust the imaging platform 20-30° so the mouse is positioned with the head slightly elevated. This position helps to ensure the optimal respiration rate for the mouse. Place the 40 MHz transducer transversely in the mounting system and carefully lower it until the front of the transducer scanhead is immersed in the ultrasound gel (**Figure 2C**).  
NOTE: Be sure to not put excessive pressure onto the mouse neck, as it could cause undue respiratory distress. In addition, it is helpful for imaging to have a buffer of gel between the transducer and the mouse.

B-Mode Imaging and Detection of Lymph Nodes:

3. Using the computer controlling the HFUS acquisition software, adjust the brightness (B-) mode settings to the following parameters: Gain 22 dB, depth 10.00 mm, width 14.08 mm.  
NOTE: These settings are a suggested starting point, and may require slight adjusting for optimal image acquisition between different applications. Observe normal cervical lymph nodes as oval hypoechoic structures near the skin surface within a surrounding hyperechoic field. The appearance of diseased lymph nodes can vary between models. To systematically image all lymph nodes within the neck region use the following steps:
  1. Use the Y-axis to scan the neck in a cranial to caudal manner towards the thoracic region. Use X-axis to center the image.
  2. Identify major landmarks: buccal cavity, tongue, and thyroid gland (**Figures 3A, B and C**; respectively); tilt the imaging platform to horizontally adjust the ventral surface of the mouse neck, making both sides of the neck appear even in the B-mode image. The amount of tilting depends upon the physiology of each individual mouse.
4. Conduct a 3D scan of the entire neck region from the buccal cavity/tongue region to the thyroid gland, in order to map lymph nodes and associated landmarks throughout the neck.
  1. Locate the tongue/buccal cavity region (**Figure 3A**) and note the numerical location on the Y scale.
  2. Locate thyroid gland (**Figure 3C**) and note the numerical location on the Y scale.
  3. Calculate the difference between the obtained values in (2.4.1) and (2.4.2) to determine the total length in mm for the imaged neck region.
  4. Use the Y knob to center the transducer on the midpoint of the determined total length.
  5. Press "3D". Enter the total length. For 3D step size, use 0.076 mm to acquire the image series stack for the entire neck region.
5. Once scanning is complete, select the right or left side of the neck and center the transducer on an individual lymph node of interest, then raise the 40 MHz transducer off the mouse. Remove the 40 MHz transducer and replace with a 50 MHz microscan transducer (also in a transverse position) to obtain higher-resolution images. Replenish the ultrasound gel on the mouse neck and lower the 50 MHz transducer into the ultrasound gel.

3D Power Doppler Imaging

6. Conduct 3D scans with power Doppler to assess volume and vascularity of individual cervical lymph nodes as follows:
  1. Press the Power button on the system keyboard to acquire power Doppler and adjust the following power-mode settings: PRF 4 KHz, Doppler gain 34 dB, 2D gain 30 dB, depth 5.00 mm, width 4.73 mm. NOTE: As before, these settings are a suggested starting point and may be modified as needed for optimal image acquisition in various models.
  2. Locate the cranial-most point of the lymph node of interest and note the location on the Y scale.
  3. Locate the most caudal point of the same node and note the location on the Y scale.
  4. Calculate the distance difference to determine the total length of the lymph node (see step 2.4.3).
  5. Center the transducer on the midpoint of the determined total length, using the Y-scale location.
  6. Press "3D" and enter total lymph node length. Use 0.051 mm for the step size.  
NOTE: Due to the proximity of the transducer to the chest region, the 50 MHz transducer may result in an unstable Doppler image due to detection of normal respiratory motion. This can be eliminated by using the "Respiration Gating" option available under the "Physiological" tab.
  7. Surround the selected lymph node with the yellow box that designates the region to be analyzed by power Doppler and select "3D scan" to acquire images. Raise the transducer off of the mouse and move it to the opposite side of the neck. Lower the transducer onto the mouse and repeat the steps described above to image lymph nodes on this side of the neck.
7. Save image sets for subsequent analysis.

### 3. Cervical Lymph Node Biopsy

1. Select the desired lymph node for biopsy and maintain HFUS imaging with the 50 MHz transducer. Choose the largest visible cervical lymph node in each side of the mouse neck. Lymph node enlargement typically indicates an inflammatory response, and therefore such nodes are ideal candidates for biopsy.  
NOTE: We have found it is very difficult to conduct biopsies on cervical nodes smaller than 10 mm<sup>3</sup>.
2. Prepare the needle and syringe for biopsy by placing a 1 ml syringe with an attached 27 G, 0.5 inch needle into the syringe holder. Adjust the needle holder to orient the needle 90° to the mouse neck (**Figure 4A**).
3. Prepare by elevating the entire mouse platform to the level of the needle. Achieve this by removing the 3D motor and switching to a taller platform, or by placing a solid object of suitable height under the provided short platform. Use a plastic microfuge tube rack for this purpose. If necessary, rotate the platform 180° in order to biopsy nodes located on the side of the neck opposite to the needle apparatus.
4. Adjust the acquisition settings by selecting "Preferences", then by choosing "Max & Extended buffer". Enlarge the field of view to a depth of 8.00 mm and width of 9.73 mm. Turn on the needle guide using the Screen Keys dial. The needle guide will predict the path of the needle on the screen and allows the user to line up the lymph node of interest in the correct location for biopsy.
5. Ensure that the lymph node remains constantly in view by centering the lymph node in the middle or slightly to the left of center in the screen (**Figure 4B**). To obtain the entire cine loop of the procedure, press Pre-trigger on the system keyboard before beginning the biopsy.
6. Adjust the needle holder until the needle tip comes into view and contacts the skin (**Figure 4B**). Advance the needle with a firm, fast push to puncture the skin. Continue to advance the needle until the tip also punctures the capsule (**Figure 4C**) and is visible within the medulla (**Figure 4D**).
7. Once the needle is properly located within the node, gently pull the syringe plunger back between the 200-300 µl demarcations to conduct the biopsy (**Figure 4D** and **4E**). Note that biopsy material is typically not visible within the syringe.
8. Gently remove the needle from the mouse neck. Expel the syringe contents into a 1.5 ml microfuge tube. Remove the needle from the syringe, leaving the needle in the tube. Collect 1 ml of biopsy media (from an aliquot, separate from the stock source) with the same syringe, and then reattach the needle to the syringe while keeping the needle in the tube.
  1. Rinse the syringe and needle with the biopsy media by expelling the biopsy media into the tube.  
NOTE: Do not pull back on the plunger while the needle is attached at any point after the biopsy. This reduces the risk of losing the biopsy material due to the small sample size.
9. Confirm lymph node content by histological means (**Figure 4F**) and analyze by additional methods (histochemistry, flow cytometry, etc.) as appropriate.
10. Once biopsy is complete, turn off the anesthesia and remove the rectal temperature probe. Remove excess ultrasound gel from mouse with gauze and remove the tape from each paw.
11. Remove the mouse from the imaging platform and return to a cage. Minimal bleeding from biopsy site may occur, but this stops without intervention. Monitor the mouse during recovery until full activity is resumed.

### 4. Image Analysis of Cervical Lymph Nodes

1. In the ultrasound software, select the image for analysis and navigate to the "Image Processing" tab. Choose "Load into 3D".
2. Select "3D Reconstructed Image" in top left corner, clicking on the "Display Single Pane" button. Use the zoom function to enlarge the image if desired. Toggle "Display Layout" to view the image only in B-mode, which removes the power Doppler overlay from view. This makes it easier to see the edges of the lymph node during subsequent 3-D analysis. Scroll through the image series to locate the beginning of the lymph node.
3. To circumscribe the lymph node, navigate to the "3D Settings" tab. Select "volume", then the "Start" button next to "Parallel".
4. Draw contours around the area of interest within individual images by scrolling. Continue until images that encompass the entire lymph node are marked. Choose "Finish" to complete the analysis.
5. At the bottom of the image, 3D volume and % vascularity will be automatically displayed.  
NOTE: 3D volume corresponds to the lymph node volume, and percent vascularity represents the percentage of the lymph node positive for blood flow by power Doppler.
6. Toggle "Display Layout" to view the power Doppler imaging as an overlay on the B- mode image. On the surface view observe a net view of the volume area of interest. Export the images in tagged image file (TIF) format or 3D scans as movies (.avi) for further use.

## Representative Results

The overall schematic for the imaging and biopsy procedures is shown in **Figure 1**. The key steps in the procedure include proper preparation of the mouse for imaging, identification of the cervical lymph nodes, correct preparation and conducting of the needle biopsy, and analysis of B-mode and Doppler images to measure volume and the amount of vascularity within each selected node using computer software.

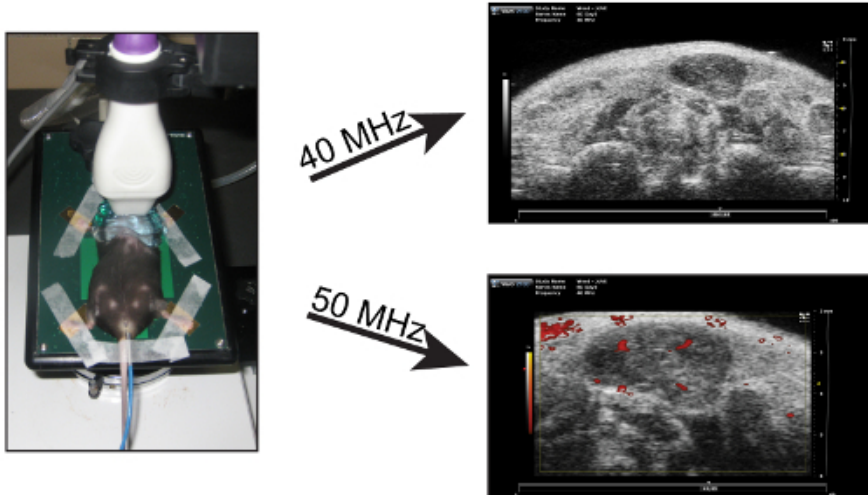
HFUS imaging of mouse cervical lymph nodes requires applying and maintaining proper anesthesia throughout the imaging period (**Figure 2A**), as well as complete removal of the hair covering the entire neck area (**Figure 2B**). The liberal application of ultrasound gel to the depilated region ensures a clear HFUS signal during the procedure (**Figure 2C**).

HFUS imaging of the neck region is aided by the visualization of cervical anatomical landmarks that produce characteristic sonographic images. **Figure 3** shows examples of the key organs (**Figure 3A-C**), cervical lymph nodes in B-mode (**Figure 3D**) and in power Doppler mode (**Figure 3E**).

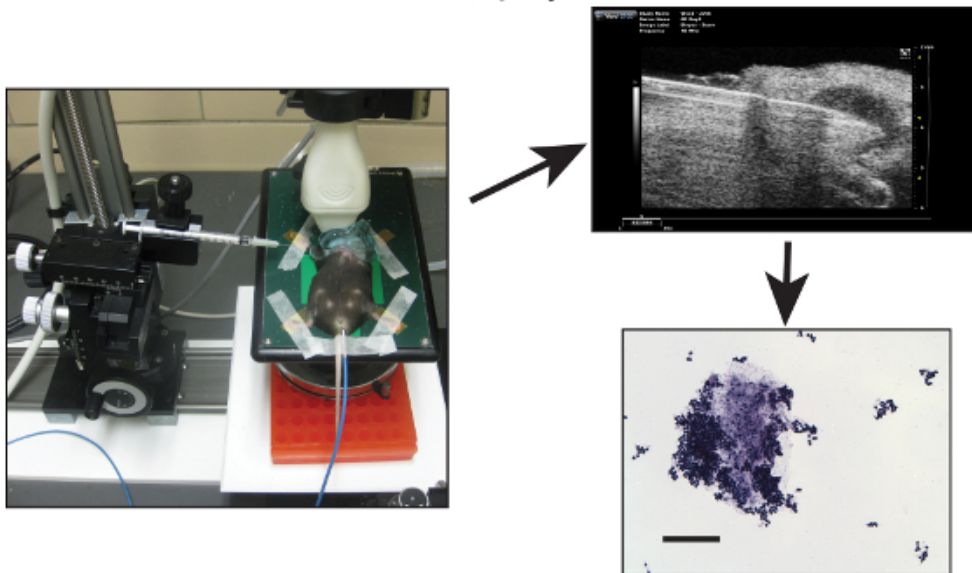
Real-time HFUS imaging in anesthetized mice allows for guided fine needle biopsy of cervical nodes similar to what is conducted in clinical practice. Placement of the biopsy needle and attached collection syringe to the controlling microinjector equipment is shown in **Figure 4A**. Subsequent B-mode sonographic images show ideal needle placement prior to biopsy (**Figure 4B**), needle tip entry into a cervical lymph node (**Figure 4C**), and needle position during biopsy (**Figure 4D**). Close-up image shows the needle tip within the medulla of the lymph node (**Figure 4E**). Processing of the biopsy components by cytopspin reveals abundant lymphoid cell clusters and associated connective tissue, verifying successful lymph node biopsy (**Figure 4F**).

Computational-based analysis of HFUS images allows for detailed information to be obtained regarding lymph node architecture, volume and vascular flow. Using power Doppler mode and 3D volume measurements, percent vascularity (PV) can be calculated from image series encompassing entire nodes (**Figure 5A**). Additionally, 3D imaging allows for virtual lymph node reconstruction, revealing overall lymph node topography (**Figure 5B**).

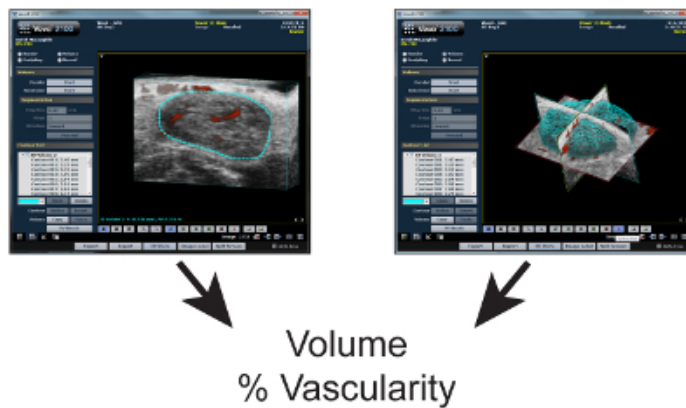
# 1. Prepare and image mouse



# 2. Biopsy



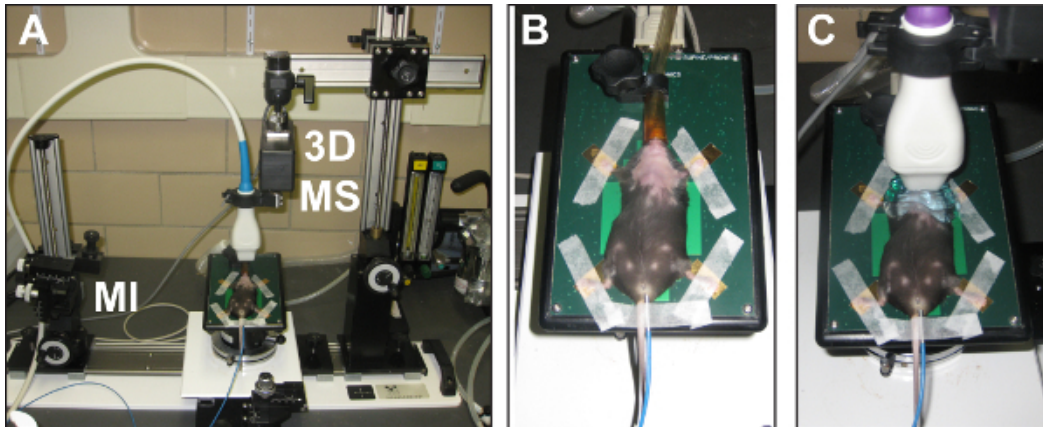
# 3. Image analysis



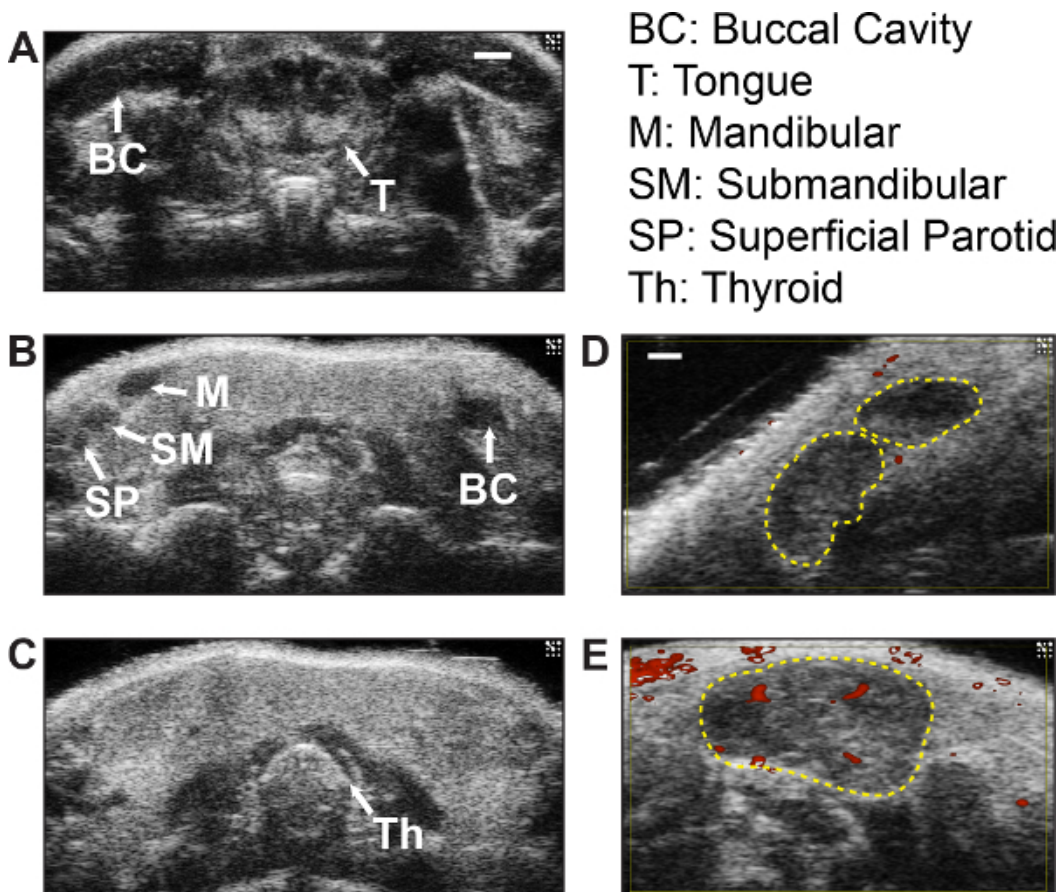
**Figure 1: Overview schematic of the steps involved in diagnostic HFUS cervical lymph node imaging in mice.** The key steps include 1: Preparing the mice for HFUS imaging and obtaining 40 and 50 MHz resolution images of the neck region containing the three mouse cervical lymph nodes. 2: Fine needle image-guided biopsy of cervical lymph nodes and subsequent histological analysis of biopsied material. 3: Computer-aided



image analysis and 3D reconstruction of lymph node images obtained in B-mode and Doppler to determine the respective lymph node volume and percent (%) of vascular flow.



**Figure 2: Overview of the high resolution *in vivo* micro-imaging system for cervical lymph node assessment and biopsy.** (A) The HFUS system is shown with an anesthetized mouse prepared for cervical lymph node imaging. Also shown is the microinjector (MI) and 3D-motor stage (3D MS) accessory equipment. (B) Close up view of an anesthetized mouse prepared for HFUS imaging with hair removed in neck region. (C) The same mouse with the 50 MHz transducer in place on the neck. Note the extra ultrasound gel used to facilitate neck region imaging.



**Figure 3: Representative HFUS cervical anatomy images in B-mode and power Doppler.** (A, B) B-mode images of the oral cavity, showing the buccal cavity (BC) and tongue (T) visualized by imaging closest to the nasal cavity. The three cervical lymph nodes found on each side of the neck (labeled M, mandibular; SM, submandibular; SP, superficial parotid), appear as a group of hypoechoic structures in a single imaging plane as shown (B). (C) The thyroid gland (Th) as visualized in the upper thoracic region, appearing as a solid, echogenic butterfly-shaped structure. (A-C) were visualized with a 40 MHz transducer; scale bar = 1 mm. (D, E) Representative images of normal (D) and enlarged (E) cervical lymph nodes with B-mode and power Doppler (red). Dotted lines outline individual lymph nodes. Scale bar = 0.5 mm.

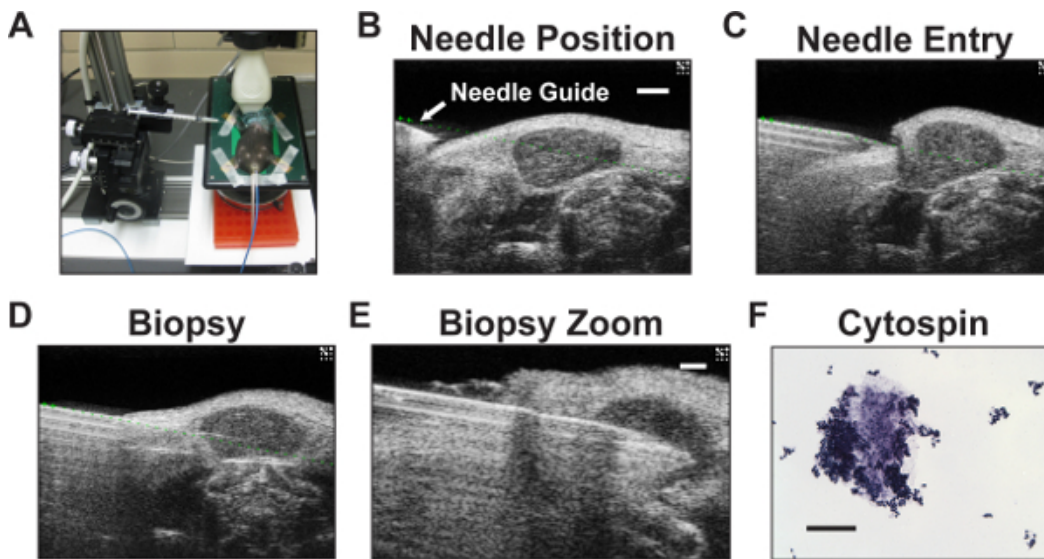


**Figure 4: Cervical lymph node biopsy set-up, imaging and cytospin analysis of biopsy material.** (A) The imaging platform showing the microinjector and needle placement near the mouse neck. A wide microcentrifuge tube rack (orange block) is used to slightly raise the platform, enabling proper needle placement while still allowing space for the 3D-motor stage. This arrangement minimizes time spent removing the motor stage for each mouse. (B-D) Whole neck HFUS images taken from a video of a cervical lymph node biopsy using the 50 MHz transducer. (B) HFUS B-mode image showing the needle positioned to the side of the neck prior to biopsy. The needle tip is the hyperechoic structure just below the position of the needle guide (green dotted line) superimposed during imaging to denote the needle trajectory. The lymph node is in the center of the image. Scale bar = 1 mm. (C) Needle entry into the lymph node. (D) Biopsy of the cervical lymph node. (E) Zoomed biopsy of cervical lymph node. Scale bar = 0.5 mm. (F) Cytospin analysis of representative biopsy lymph material confirming successful biopsy. Scale bar = 100  $\mu$ m.

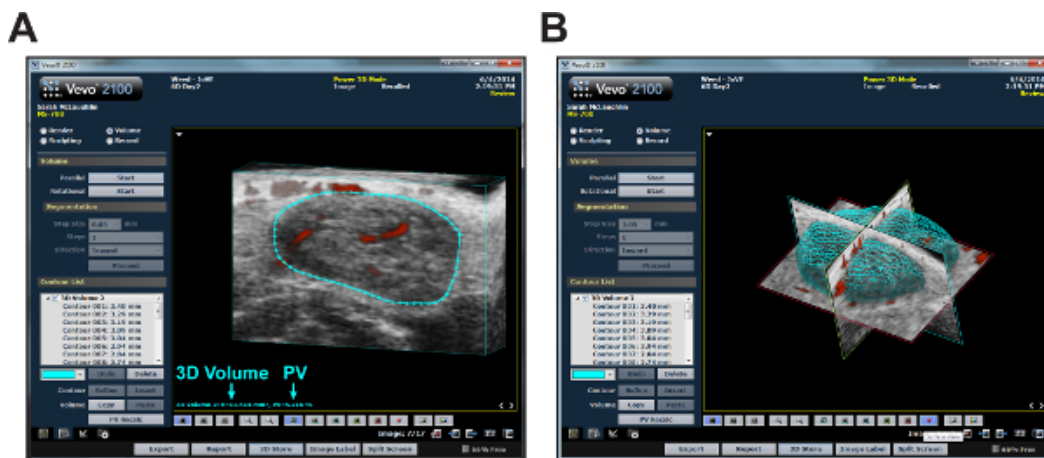


**Figure 5: Computer analysis of 3D cervical lymph node images.** (A) Representative screenshot of a lymph node analyzed using computer software. The node is circumscribed in blue; analysis results show 3D Volume and percent vascularity (PV) as indicated. (B) A surface view image of the same node after 3D analysis. Renders entire volume of lymph node based on measurements taken in A.

## Discussion

The described protocol allows for the visualization and in situ evaluation of murine cervical lymph nodes using non-invasive HFUS imaging. The use of B-mode and power Doppler imaging to visualize cervical lymph node morphology, volume and lymph node blood flow provides for an experimental analysis of preclinical mouse model systems similar to that used for the characterization of cervical patient nodes in clinical practice. The ability to monitor the cervical lymph nodes via fine needle biopsy also provides a useful technique for detecting immune cell alterations and the presence of foreign cell types or bacteria during oral cavity disease-induced lymphadenopathies in mice. The ease of use and low cost associated with HFUS allows for the rapid screening of cervical lymph node status in a wide variety of animal models.

A critical step in this protocol is the initial successful identification of the cervical lymph nodes in HFUS images. Our facility has an assortment of HFUS transducers as described, so we have used them to obtain the highest quality images. However, if the transducers we describe are unavailable, it is possible to adapt the imaging using other transducers. For this purpose, adjusting image depth and width to obtain an adequate image is all that is required. Resolution of such images may vary, but it should still be possible to obtain high quality images by using HFUS. Imaging landmarks of the oral cavity and the thyroid gland will greatly aid in orienting the user to the proper region where the lymph nodes are localized. The characteristic oval-shaped, hypoechoic nature and superficial location close to the skin surface allows for rapid confirmatory identification of the cervical lymph nodes within the proper neck region. While all three nodes may be visible in a single imaging plane (Figure 3B),

typically one or two nodes are captured during imaging. Minor adjustments of the transducer position can be conducted to render different imaging planes visible, allowing visualization of all nodes on a single side of the neck.

While we have found the described technique reliable for identifying cervical lymph nodes, there are specific limitations to the imaging and biopsy technique. The superficial nature of mouse cervical lymph nodes confers excessive mobility when even slight pressure is applied to the skin via the transducer head. This can be counteracted by slowly applying the transducer head into the ultrasound gel on the mouse neck until the landmark images are identified. Lymph node mobility can also complicate the fine needle biopsy, especially when using transducers in the higher resolution (50 MHz) range. Centered images of lymph nodes for biopsy are typically pushed out of the field of view due to the force of the biopsy needle needed to puncture the overlying skin and capsule. This can be remedied by the off-center positioning of the lymph node towards the direction of needle entry, providing space for the lymph node to be pushed across but still remain within the field of view during biopsy. In our experience, lymph nodes >10 mm<sup>3</sup> are very difficult to biopsy, and are often pushed by the needle rather than penetrated during needle advancement. Thus, biopsy is best reserved for enlarged lymph nodes where the size is >10 mm<sup>3</sup> to ensure sufficient node target size and stability within the cervical region. In addition, biopsy material may not contain sufficient cell numbers for procedures where larger cell numbers are required (e.g., flow cytometry).

HFUS has been used to successfully visualize orthotopic HNSCC tumors<sup>25</sup>, and has the potential to monitor cervical node metastasis in mice with oral tumors<sup>24</sup>. In addition to ultrasound, bioluminescence imaging has also been used to visualize orthotopic oral tumor formation and cervical lymph node metastasis in live mice<sup>26,27</sup>. As an alternative approach, bioluminescence imaging has a distinct advantage over HFUS in being able to directly quantify tumor progression and metastatic burden over time in the same animal. While undeniably useful, bioluminescence imaging is unable to measure many of the parameters visualized by HFUS, including lymph node morphology, nodal volumes or blood flow. Bioluminescence imaging also requires specialized dark boxes to maintain mice during imaging, rendering this technique unsuitable for adaptation for fine needle biopsy.

Furthermore, bioluminescence imaging requires production of tumor cells that stably express the luciferase enzyme, allowing this technique to be used only in cases of orthotopic xenografts with luciferase-transfected tumor cells in immunocompromised mice, or with inducible tissue-specific transgenic systems that restrict luciferase expression in a spatio-temporal manner specific to the tissue of tumor origin. In contrast, HFUS can be used in conjunction with bioluminescence images in these models, as well as being capable of imaging cervical lymph nodes in models of carcinogen-induced oral tumors in mice with complete immune systems<sup>28,29</sup>. While HFUS may be more adaptable to most mouse models of oral cancer, the combined information that can be obtained from bioluminescence and HFUS imaging in systems where tumor cells express luciferase can provide a more complete picture of cervical lymph node involvement than either imaging modality alone.

The ability to identify and detect mouse cervical lymph nodes in real time allows for this technique to be used in most models of oral disease that result in inflammatory lymphadenopathy where the animal can be maintained in an inverted position under short-term anesthesia. Detection of lymph node metastasis or bacterial infection and the concomitant impact on lymph node morphology in living animals presents a significant benefit over traditional methods that require lymph nodes to be removed from dead animals for histological processing. Combining HFUS with fine needle biopsy allows a means for conducting routine pathological analysis of cervical lymph nodes, similar to what is conducted in the clinic, providing an improved method for monitoring disease progression in most current mouse models of oral cavity diseases.

## Disclosures

Publication costs for this article are sponsored by Visual Sonics.

## Acknowledgements

This work was supported by Dorothy D. Radford Endowment fund from the West Virginia University Mary Babb Randolph Cancer Center. The use of the West Virginia University Animal Models and Imaging Facility (AMIF) and Microscopy Imaging Facility (MIF) (supported by the Mary Babb Randolph Cancer Center and NIH grants P20 RR16440, P30 RR032138/GM103488 and S10 RR026378) is gratefully acknowledged.

## References

1. Montone, K. T. Infectious diseases of the head and neck: a review. *Am J Clin Pathol.* **128**, (1), 35-67 (2007).
2. Bryson, T. C., Shah, G. V., Srinivasan, A., Mukherji, S. K. Cervical lymph node evaluation and diagnosis. *Otolaryngol Clin North Am.* **45**, (6), 1363-1383 (2012).
3. Joshi, P. S., Pol, J., Sudesh, A. S. Ultrasonography - A diagnostic modality for oral and maxillofacial diseases. *Contemp Clin Dent.* **5**, (3), 345-351 (2014).
4. Oz, F., et al. Evaluation of clinical and sonographic features in 55 children with tularemia. *Vector Borne Zoonotic Dis.* **14**, (8), 571-575 (2014).
5. Niedzielska, G., Kotowski, M., Niedzielski, A., Dybiec, E., Wiczorek, P. Cervical lymphadenopathy in children—incidence and diagnostic management. *Int J Pediatr Otorhinolaryngol.* **71**, (1), 51-56 (2007).
6. Ying, M., Bhatia, K. S., Lee, Y. P., Yuen, H. Y., Ahuja, A. T. Review of ultrasonography of malignant neck nodes: greyscale, Doppler, contrast enhancement and elastography. *Cancer Imaging.* **13**, (4), 658-669 (2013).
7. Stoeckli, S. J., et al. Initial staging of the neck in head and neck squamous cell carcinoma: a comparison of CT, PET/CT, and ultrasound-guided fine-needle aspiration cytology. *Head Neck.* **34**, (4), 469-476 (2012).
8. Rottey, S., et al. Evaluation of metastatic lymph nodes in head and neck cancer: a comparative study between palpation, ultrasonography, ultrasound-guided fine needle aspiration cytology and computed tomography. *Acta Clin Belg.* **61**, (5), 236-241 (2006).
9. Greco, A., et al. Ultrasound biomicroscopy in small animal research: applications in molecular and preclinical imaging. *J Biomed Biotechnol.* **2012**, (2012).
10. Chen, J. J., Fu, S. Y., Chiang, C. S., Hong, J. H., Yeh, C. K. Characterization of tumor vasculature distributions in central and peripheral regions based on Doppler ultrasound. *Med Phys.* **39**, (12), 7490-7498 (2012).



11. El Kaffas, A., Giles, A., Czarnota, G. J. Dose-dependent response of tumor vasculature to radiation therapy in combination with Sunitinib depicted by three-dimensional high-frequency power Doppler ultrasound. *Angiogenesis*. **16**, (2), 443-454 (2013).
12. Bachawal, V. S. Earlier detection of breast cancer with ultrasound molecular imaging in a transgenic mouse model. *Cancer Res*. **73**, (6), 1689-1698 (2013).
13. Loveless, M. E., et al. A method for assessing the microvasculature in a murine tumor model using contrast-enhanced ultrasonography. *J Ultrasound Med*. **27**, 12-1699 (2008).
14. Snyder, C. S., et al. Complementarity of ultrasound and fluorescence imaging in an orthotopic mouse model of pancreatic cancer. *BMC Cancer*. **9**, 106 (2009).
15. Kodama, T., et al. Volumetric and angiogenic evaluation of antitumor effects with acoustic liposome and high-frequency ultrasound. *Cancer Res*. **71**, (22), 6957-6964 (2011).
16. Hwang, M., Hariri, G., Lyshchik, A., Hallahan, D. E., Fleischer, A. C. Correlation of quantified contrast-enhanced sonography with in vivo tumor response. *J Ultrasound Med*. **29**, (4), 597-607 (2010).
17. Li, L., Mori, S., Sakamoto, M., Takahashi, S., Kodama, T. Mouse model of lymph node metastasis via afferent lymphatic vessels for development of imaging modalities. *PLoS One*. **8**, (2), e55797 (2013).
18. Springer, D. A., et al. Investigation and identification of etiologies involved in the development of acquired hydronephrosis in aged laboratory mice with the use of high-frequency ultrasound imaging. *Pathobiol Aging Age Relat Dis*. **4**, (2014).
19. Papadopoulos, G., et al. A Mouse Model for Pathogen-induced Chronic Inflammation at Local and Systemic Sites. *J Vis Exp*. (90), (2014).
20. Vulcano, A. B., et al. Oral infection with enteropathogenic *Escherichia coli* triggers immune response and intestinal histological alterations in mice selected for their minimal acute inflammatory responses. *Microbiol Immunol*. **58**, (6), 352-359 (2014).
21. Myers, J. N., Holsinger, F. C., Jasser, S. A., Bekele, B. N., Fidler, I. J. An orthotopic nude mouse model of oral tongue squamous cell carcinoma. *Clin Cancer Res*. **8**, (1), 293-298 (2002).
22. Kanojia, D., Vaidya, M. M. 4-nitroquinoline-1-oxide induced experimental oral carcinogenesis. *Oral Oncol*. **42**, (7), 655-667 (2006).
23. Van den Broeck, W., Derore, A., Simoens, P. Anatomy and nomenclature of murine lymph nodes: Descriptive study and nomenclatory standardization in BALB/cAnNCrl mice. *J Immunol Methods*. **312**, (1-2), 12-29 (2006).
24. Walk, E. L., McLaughlin, S., Coad, J., Weed, S. A. Use of high frequency ultrasound to monitor cervical lymph node alterations in mice. *PLoS One*. **9**, (6), e100185 (2014).
25. Pezold, J. C., Zinn, K., Talbert, M. A., Desmond, R., Rosenthal, E. L. Validation of ultrasonography to evaluate murine orthotopic oral cavity tumors. *ORL J Otorhinolaryngol Relat Spec*. **68**, (3), 159-163 (2006).
26. Sano, D., Myers, J. N. Metastasis of squamous cell carcinoma of the oral tongue. *Cancer Metastasis Rev*. **26**, (3-4), 645-662 (2007).
27. Sano, D., et al. The effect of combination anti-endothelial growth factor receptor and anti-vascular endothelial growth factor receptor 2 targeted therapy on lymph node metastasis: a study in an orthotopic nude mouse model of squamous cell carcinoma of the oral tongue. *Arch Otolaryngol Head Neck Surg*. **135**, (4), 411-420 (2009).
28. Tang, X. H., Knudsen, B., Bemis, D., Tickoo, S., Gudas, L. J. Oral cavity and esophageal carcinogenesis modeled in carcinogen-treated mice. *Clin Cancer Res*. **10**, (1 Pt 1), 301-313 (2004).
29. Vitale-Cross, L., et al. Chemical carcinogenesis models for evaluating molecular-targeted prevention and treatment of oral cancer. *Cancer Prev Res (Phila)*. **2**, 419-422 (2009).